

# Green synthesis of gold nanoparticles from *Dendrobium officinale* and its anticancer effect on liver cancer

Wei Zhao<sup>a</sup>, Ji Li<sup>b</sup>, Cheng Zhong<sup>c</sup>, Xuyu Zhang<sup>c</sup> and Yixi Bao<sup>c</sup>

<sup>a</sup>Department of Oncology, The Second Affiliated Hospital of Chongqing Medical University, Chongqing, PR China; <sup>b</sup>Department of Thoracic Surgery, Chongqing Public Health Medical Center, Chongqing, PR China; <sup>c</sup>Department of Clinical Laboratory, The Second Affiliated Hospital of Chongqing Medical University, Chongqing, China

## ABSTRACT

A novel gold nanoparticle (Do-AuNP) was successfully synthesized from water extracts of traditional Chinese medicine *Dendrobium officinale* (DO) without using any extra chemicals reagents. The physico-chemical properties of Do-AuNPs were analyzed by transmission electron microscopy, dynamic light scattering, energy-dispersive X-ray spectroscopy, Fourier transform infrared spectroscopy, and atomic force microscopy. The amount of DO extract on the AuNPs was about 13%. In order to evaluate the anti-tumor efficiency and biosafety, the inhibitory rate of HepG2 cells and survival rate of L02 cells were performed *in vitro*, and the immunohistochemical analysis of H&E, Ki-67, and TUNEL staining were conducted *in vivo*. Our results demonstrated that Do-AuNP had better anti-tumor efficiency compared with DO extraction alone without increasing toxicity *in vivo* and *in vitro*. The present study provides useful information for Do-AuNP as a new nanomedicine for liver cancer.

## ARTICLE HISTORY

Received 26 March 2021  
Revised 18 April 2021  
Accepted 20 April 2021

## KEYWORDS

*Dendrobium officinale*; gold nanoparticles; biosafety; liver cancer



## 1. Introduction

In recent years, there has been an increase in the use of nanomaterials in the field of medicine. Gold nanoparticles (AuNPs) possess remarkable optical, plasma resonance, and bioconjugation properties, which facilitate high stability and can be easily combined with biological molecules (Liu et al., 2019). Thus, AuNPs are widely used in the biomedical industry, including the fields of clinical chemistry, immunology, microbiology, and cancer (El-Sayed et al., 2005; Medley et al., 2008; Bagheri et al., 2018). Additionally, AuNPs are also used in the diagnosis and treatment of malignant tumors (El-Sayed et al., 2005; Medley et al., 2008; Bagheri et al., 2018; Khan & Khan, 2018). However, the nanoparticles synthesized by physical and chemical methods have been shown to exhibit low efficacy and toxic by-products. Therefore, there is an urgent need to develop novel methods for the synthesis of nanoparticles with minimally toxic side products.

Traditional Chinese medicine (TCM) is known for its good efficacy and minimal side effects. Researchers often use modern medical techniques to purify the components present in TCM, such as polysaccharides, phenolic acids, flavonoids, esters, and coumarins, and then analyze their individual pharmacological activities, including immunological benefits, anti-infection, and anti-tumor activities, etc. (Yu et al., 2018; Teng et al., 2020). *Dendrobium officinale* (*Dendrobium officinale* Kimura et Migo, DO) is a widely used TCM, which is known to exhibit various pharmacological activities, such as

intestinal immunity regulation (Xie et al., 2016), anti-tumor (Li et al., 2019; Liang et al., 2019), and metabolic regulation in diabetes (Yang et al., 2020). Some studies have shown that DO exerts an inhibitory effect on liver cancer (Xing et al., 2018a,b). Here, we performed water extraction of DO to synthesize AuNPs and study their biological activities to avoid the use of toxic and harmful chemical reagents in the process of drug separation.

According to the Global Cancer Statistics 2021, the incidence of liver cancer has stabilized in men; however is on a steady rise (2% annually) in women, mainly due to obesity, hepatitis B virus, and hepatitis C virus, etc. (Siegel et al., 2021). Currently, the primary treatment of liver cancer involves surgical resection; however, most patients are diagnosed late and thus, cannot undergo surgical resection (Forner et al., 2018). Although Solafinib has shown significant efficacy for the systemic treatment of liver cancer, the survival rate is less than 3 months (Keating, 2017). Transarterial chemoembolization (TACE) has been shown to be effective in patients with advanced, unresectable liver cancer (Lo et al., 2002). Recent studies have shown the beneficial effects of the use of immunotherapy drugs, such as nivolumab, atezolizumab with or without bevacizumab for the treatment of liver cancer (Yau et al., 2019; Lee et al., 2020; Pinato et al., 2020; Yang et al., 2020). However, the available treatment methods have limited efficacy, high recurrence rate, and are prone to distant metastasis. Thus, there is an urgent need to develop novel methods for the treatment of liver cancer.

**CONTACT** Yixi Bao  [yixibao@cqmu.edu.cn](mailto:yixibao@cqmu.edu.cn)  Department of Clinical Laboratory, The Second Affiliated Hospital of Chongqing Medical University, No. 74 Linjiang Road, Yuzhong District, Chongqing, China

© 2021 The Author(s). Published by Informa UK Limited, trading as Taylor & Francis Group.

This is an Open Access article distributed under the terms of the Creative Commons Attribution-NonCommercial License (<http://creativecommons.org/licenses/by-nc/4.0/>), which permits unrestricted non-commercial use, distribution, and reproduction in any medium, provided the original work is properly cited.

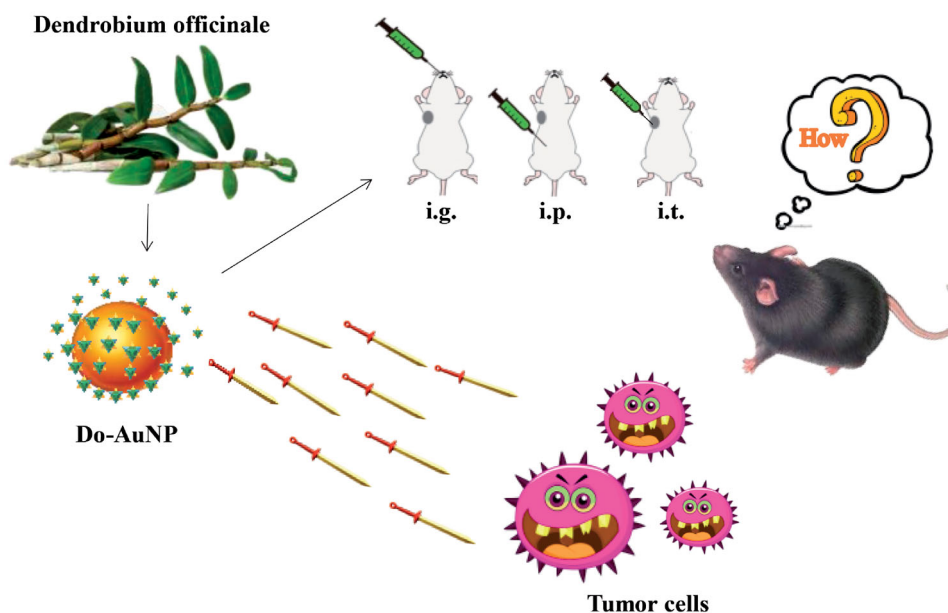


**Figure 1.** Conceptual diagram of Do-AuNP effect *in vitro* and *in vivo* (intragastric gavage (i.g.), intraperitoneal (i.p.), or intratumoral injection (i.t.)).

Recently, several studies have shown that green synthesis of AuNPs from TCM extracts, such as *Rabdosia rubescens* Linn, Siberian ginseng, banana peel, etc., has inhibitory effects on tumor cells (Wu et al., 2019; Zhang et al., 2019; Liu et al., 2020). Since DO has been reported to have effect on anti-cancer and immune regulation in liver cancer as mentioned above and maybe we would be able to enhance the bioavailability of DO by combining it with AuNPs. Therefore, in this study, we synthesized AuNPs from DO extract (Do-AuNP) and explored its effect on liver cancer, which might provide a new strategy for the treatment of liver cancer (Figure 1).

## 2. Materials and methods

### 2.1. Materials

*Dendrobium officinale* was purchased from the herbal medicine market in Chongqing, China and was authenticated by Professor Xiaojun Sun from Beijing Huadafangke Commodity Quality Inspection Co. Ltd. (Beijing, China) before the preparation of AuNPs. Adriamycin (ADM) was obtained from Shenzhen Main Luck Pharmaceuticals Inc. (Shenzhen, China). Chloroauric acid ( $\text{HAuCl}_4$ ) was purchased from Shanghai Xianding Biological Technology Co. Ltd. (Shanghai, China). Trisodium citrate dihydrate was gained from Beijing G-CLONE Biological Technology Co. Ltd. (Beijing, China). The cell counting kit-8 (CCK-8) assay kit was purchased from Boster Biological Technology Co. Ltd. (Pleasanton, CA). Dulbecco's modified Eagle's medium (DMEM) and 0.25% EDTA/trypsin were procured from HyClone (Logan, UT). Fetal bovine serum (FBS) was purchased from Gibco Life Technologies (Carlsbad, CA).

### 2.2. Preparation of *Dendrobium officinale* extract

We boiled DO powder (100g) for 2 h at 80 °C in 1 L of distilled water. The extract was filtered and concentrated in a

rotary evaporator. Then, the extract was freeze-dried to yield the fine powder for further analysis.

### 2.3. Synthesis of Do-AuNP

*Dendrobium officinale* gold nanoparticles (Do-AuNP) were synthesized by adding 2.4 mg/mL of DO to 1 mM chloroauric acid and incubated at 80 °C for 30 min. The synthesis of Do-AuNPs was confirmed based on the change in the color of the solution from light yellow to wine red (Wu et al., 2019). The UV spectroscopic analysis was done to further confirm the properties of Do-AuNP. Besides, Au nanoparticle without DO was synthesized according to the method of another study (Haiss et al., 2007).

Moreover, the absorbance value of DO extract at different concentrations (0.2, 0.4, 0.6, 0.8, and 1.0 mg/mL) were measured by ultraviolet spectrophotometer at 540 nm to prepare the standard curve of DO extract. The Do-AuNPs nanoparticles were collected by high-speed centrifugation for 30 min, and the weight ( $m_1$ ) of nonabsorbent DO in the supernatant was measured by the standard curve. The weight of DO attached to the AuNPs' surface was obtained by subtracting  $m_1$  from the total mass ( $m_0$ ) we added to the solution. Then, the precipitation was lyophilized and weighed as  $m_2$ . In total, the amount of DO extract on the AuNPs was calculated as  $(m_0 - m_1)/m_2$ .

### 2.4. Cell counting kit-8 assay

HepG2 and L02 were gifted by the Key Laboratory of Molecular Biology for Infectious Diseases of the Second Affiliated Hospital of Chongqing Medical University. HepG2 and L02 cells were cultured in DMEM medium, supplemented with 10% FBS, 100 U/mL penicillin, and 100 µg/mL streptomycin in a CO<sub>2</sub> incubator at 37 °C.

The HepG2 and L02 cells ( $5 \times 10^3$  cells/well) were seeded in 96-well plates. Next, various concentrations of DO and

Do-AuNPs (50, 100, 200, and 400  $\mu\text{g}/\text{mL}$ ) were added after adhesion. Also, NS and ADM (2  $\mu\text{g}/\text{mL}$ ) were added as negative and positive controls. After 24 h of culture, CCK-8 reagent (10  $\mu\text{L}/\text{well}$ ) was added to every well and incubated for 1.5 h. Finally, the cell viability was evaluated in both cell lines using UV-Vis spectrophotometer by OD values (450 nm), respectively. All assays were performed thrice. The results were defined as follows (Long et al., 2018):

$$\text{Cell viability (\%)} = \frac{[\text{OD}(\text{experiment}) - \text{OD}(\text{blank})]}{[\text{OD}(\text{control}) - \text{OD}(\text{blank})]} \times 100\%.$$

$$\begin{aligned} \text{Cell proliferation inhibition rate (\%)} \\ = \frac{[\text{OD}(\text{control}) - \text{OD}(\text{experiment})]}{[\text{OD}(\text{control}) - \text{OD}(\text{blank})]} \times 100\%. \end{aligned}$$

## 2.5. Animals and tumor model

Female C57BL/6 mice (age: 6–8 weeks) were purchased from the Animal Facility of Chongqing Medical University. After one week of acclimatization, we established a tumor model by subcutaneously injecting cultured mouse hepatocellular carcinoma tumor strains, H22 tumor cells ( $4 \times 10^5$  cells/mouse), into the right armpit of mice. The mice were returned to the original environment with standard feeding for 10 days after the injection and were randomly divided into nine groups ( $n=6$  each). The mice were treated with 2 mg/kg DO and Do-AuNP by an intragastric gavage (i.g.), intraperitoneal (i.p.), or intratumoral (i.t.) injection daily for 3 weeks; saline was used as the control.

We used a caliper to record body weights and tumor sizes every two days; the tumor volume was calculated using the following formula:  $(a \times b^2)/2$ , where  $a$  and  $b$  represent the longest and shortest diameter of the tumor, respectively (Zou et al., 2019). The mice were sacrificed by cervical dislocation, and tumors, spleen, liver, heart, lungs, kidney, thymus, and peripheral blood samples were collected. The organ index and the tumor inhibition rate were calculated using the following formulas:

$$\text{Organ index} = \frac{\text{spleen}(\text{thymus})\text{weight}}{\text{body weight}} \times 10 \times 100\%,$$

$$\text{Tumor inhibition rate} = [1 - A/B] \times 100\%$$

where  $A$  is the weight of the tumors of the treated groups and  $B$  is the weight of the tumors of the NS group.

All tumors were fixed with 4% polyoxymethylene for hematoxylin and eosin (H&E) staining, terminal deoxynucleotidyl transferase-mediated dUTP-biotin nick end labeling (TUNEL), and antigen Ki67. The images were visualized using a Nikon E100 microscope and Nikon DS-U3 camera (Nikon, Minato, Japan). The percentage of total positive cells was calculated by randomly recording three fields at  $\times 200$  magnification.

## 2.6. Statistical analysis

The data were expressed as average  $\pm$  SD and all analyses were conducted in triplicate. Comparison between multiple groups was assessed with the  $t$ -test, and one-way analysis of variance (ANOVA) followed by Student's Newman-Keuls post hoc test. These variables were repeatedly measured at different time points in order to analyses and  $p < .05$  was considered statistically significant.

## 3. Results and discussion

### 3.1. Synthesis and characterization of Do-AuNPs

#### 3.1.1. Ultraviolet-visible spectroscopy

There has been a rapid development in the green synthesis of nanoparticles from Chinese herbal drugs in multiple medical fields (Markus et al., 2017). According to the experience from other previous studies, the synthesis of Do-AuNPs could be confirmed by color change of red wine (Venkatesan et al., 2014) and ultraviolet-visible (UV) spectroscopic analysis. Figure 2(A) shows the maxima of the absorbance peak was detected at approximately 540 nm due to the surface plasmon resonance property of gold, which also correlates with the study of Rui (Liu et al., 2019) that states the nanoparticles of spherical shape they synthesized showed a strong absorption at 530 nm and decreasing after 600 nm. Besides, the peak absorbance in the UV analysis was found to be consistent with time for 30 days (Figure 2(A)), which indicated the stability of Do-AuNP. Besides, the corresponding mass was measured as  $m_0$  (1.44 mg),  $m_1$  (0.86 mg), and  $m_2$  (4.518 mg), then the amount of DO extract on the AuNPs was calculated as 13% by the methods mentioned above.

#### 3.1.2. Particle size analysis

Figure 3(A) shows the transmission electron microscopic (TEM) image of Do-AuNPs, which was not uniform in size with a spherical shape; the average size of biosynthesized Do-AuNPs was measured to be 30 nm or so which were larger compared with Au nanoparticles alone. The dynamic light scattering (DLS) analysis of Do-AuNPs confirmed the

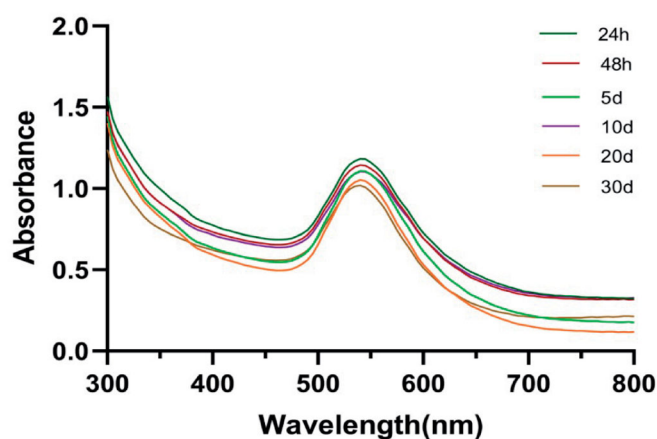
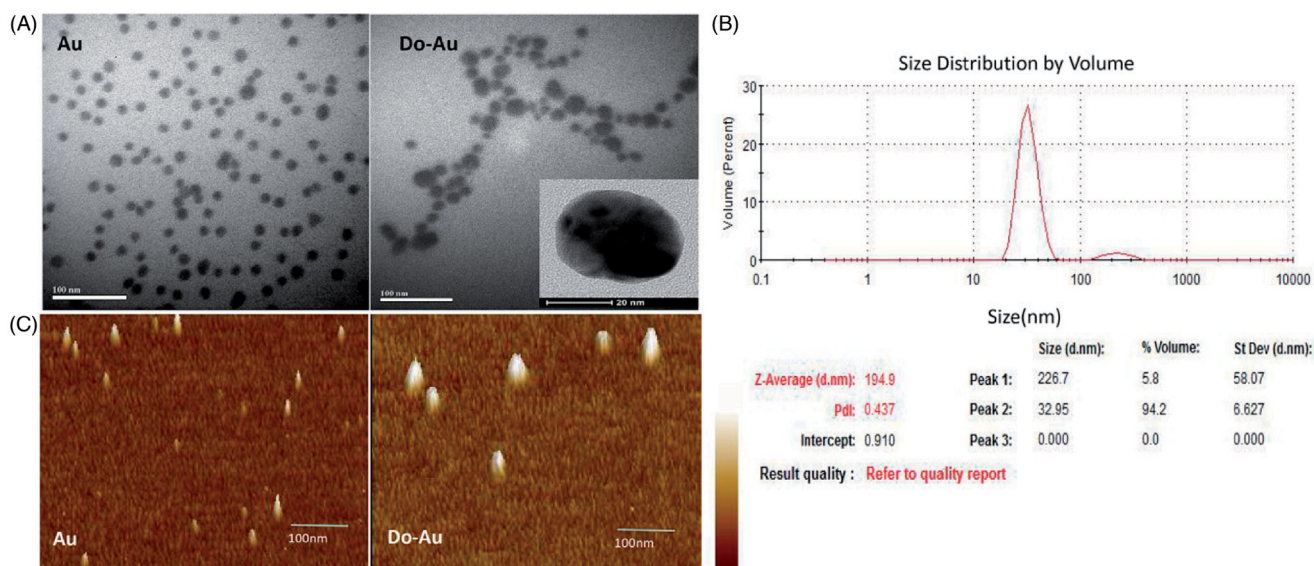


Figure 2. The UV-visible spectrum absorption pattern of Do-AuNP at different time.



**Figure 3.** Particle size of Do-AuNP (A) photograph of high resolution transmission electron microscopy (TEM). (B) Dynamic light scattering (DLS) analysis. (C) Atomic force microscopy analysis (AFM).

size to be 32.95 nm in diameter which were also larger than Au nanoparticles alone (Figure 3(B)). The polydispersity value of Do-AuNPs was reported to be 0.437 which might have also indicated a good distribution of these particles. The results of DLS analysis corresponded with those of TEM which indicated the composition of Do-AuNPs and their unequal sizes. The non-uniform size distribution of Do-AuNPs was in correlation with the fact that the herbal extraction particles were not equivalent because of the variable composition of DO. In other words, when the AuNPs were coated with different herbal extraction particles, they formed particles of uneven size. Based on DLS analysis, the main peak of Do-AuNPs curve representing the average volume of most particles was distributed around 32.95 nm. Thus, in conclusion, the particle size of Do-AuNPs was defined as approximately 30 nm.

In addition, we used an atomic force microscope (AFM) to observe the surface morphology of Do-AuNPs (Figure 3(C)). As shown in the figure, the surface of the Au particles is smooth and the particle size is about 10 nm. However, the top of the Do-AuNPs particle surface is relatively rough and the particle size is non-normally distributed. The above results are consistent with the TEM, which further indicates that Do is successfully attached to the surface of AuNPs.

*Dendrobium officinale* extract has been reported to cross cell membranes easily and inhibit the growth of HepG2 cancer cells (Xing et al., 2018a). In addition, some studies have shown that AuNPs were well applied in drug delivery targeting into cells and effectively release drugs (Donoso-González et al., 2021). In our study, the Do-AuNPs significantly increased the contact area of drugs, and we supposed that they are able to target to tumor cells with higher loading efficiency and increase the bioavailability.

### 3.1.3. Composition of Do-AuNPs

The active biomolecules present in the biosynthesized Do-AuNPs were evaluated by Fourier transform infrared

spectroscopy (FTIR) (Figure 4(A)). The main characteristic peaks were observed between 1000 and 3500  $\text{cm}^{-1}$ . The peaks at 3409.03  $\text{cm}^{-1}$  corresponded to the stretching vibration peak of the phenolic isohydroxyl group (AROH). The absorption peaks measured at 2928  $\text{cm}^{-1}$  and 1731.92  $\text{cm}^{-1}$  were the stretching vibration peak of the alkyl group and the carbonyl group, respectively. The peak at 1640  $\text{cm}^{-1}$  was due to the stretching of the double bond (C=C AR). The peaks between 1060 and 1030  $\text{cm}^{-1}$  were the out-of-plane vibration peaks of the aromatic hydrogen (ARH). Additionally, the peaks between 1249 and 1427  $\text{cm}^{-1}$  were the in-plane vibration peak of alkyl hydrogen.

The original method of reducing AuNPs involved chemical, electrochemical, and photolytic reduction techniques (Pestov et al., 2016). The reduction involved functional groups, such as hydrosulfonyl (-SH) and aldehyde group (-CHO) (Zhang et al., 2019). Studies on the components of DO identified polysaccharides, alkaloids, amino acids, esters, alcohols, flavonoids, glycosides, etc. (Zhou et al., 2018; Hu et al., 2020). In this study, the FTIR analysis of Do-AuNPs showed a peak at 1640.98  $\text{cm}^{-1}$ , 1731.92  $\text{cm}^{-1}$ , and 2928  $\text{cm}^{-1}$ , which not only indicated the existence of esters and aromatic compounds, but also supported the possible underlying mechanisms of DO extract to reduce chloroauric acid to synthesize Do-AuNPs.

Figure 4(B) shows the energy dispersive X-ray analysis (EDAX) results of Do-AuNPs which indicated the composition elements. A few peaks around 10 keV were observed, which suggested the presence of Au ions in the Do-AuNPs, and a strong peak was measured at 7 keV, indicating the presence of Cu atoms, which could be a part of the supporting filament made of copper grids.

### 3.2. CCK-8 assay

The CCK-8 assay was performed to evaluate the biocompatibility of the Do-AuNPs. HepG2 and L02 cell lines were originated from human hepatocellular carcinoma cells and

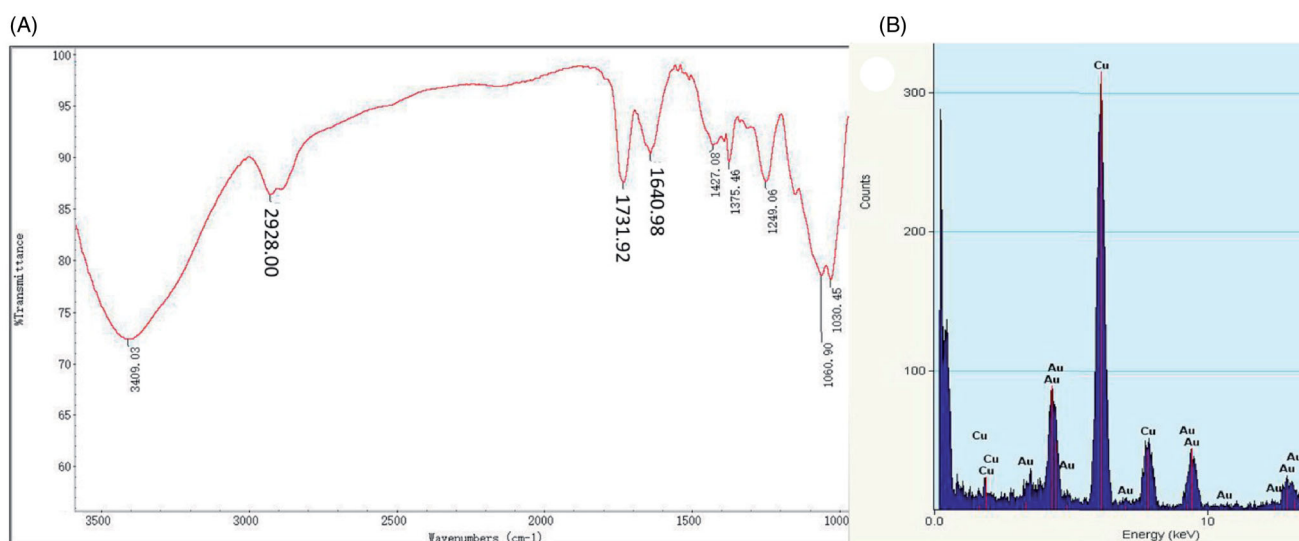


Figure 4. FTIR and EDAX of Do-AuNP (A) FTIR and (B) energy dispersive X-ray analysis (EDAX).

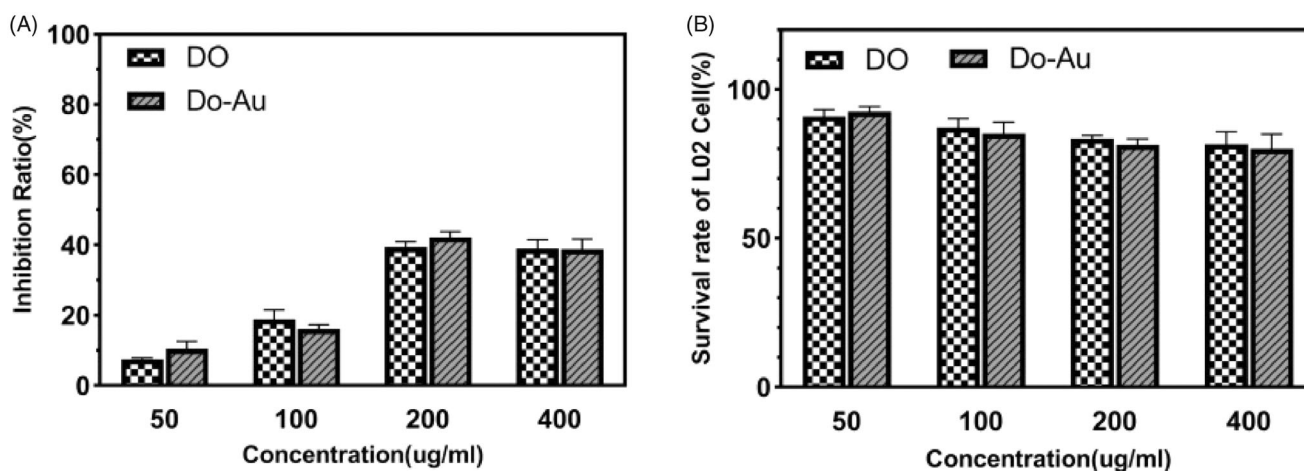


Figure 5. The cellular assays of Do-AuNP. (A) The inhibition rates of Do and Do-AuNP at various concentrations on HepG2 cells. (B) The survival rates of Do and Do-AuNP at various concentrations on L02 cells.

normal liver cells, respectively. After the treatment with different concentrations of DO and Do-AuNPs, the viability of HepG2 cells was found to significantly reduce in a dose-dependent manner (Figure 5(A)). Both drugs showed a high inhibition rate on HepG2 cells at 200  $\mu\text{g}/\text{mL}$ , but the effect of Do-AuNPs was slightly better. In addition, both drugs had little effect on the survival rate of normal liver cells (L02) indicating that the Do-AuNPs had good biocompatibility (Figure 5(B)).

The reason why there is no significant difference in the inhibitory effect on HepG2 between Do-AuNP and Do alone *in vitro* might be that the active ingredients were DO extract which encapsulated the AuNPs in it. However, its pharmacokinetics might change due to the addition of AuNPs *in vivo*, thus increasing the anti-tumor effect significantly.

### 3.3. Tumor inhibition in vivo

#### 3.3.1. Weight and volume

In the *in vivo* assay, we injected mouse liver cancer cells (H22) directly into the right armpit of mice to establish a

classic subcutaneous liver tumor model. The grouping and administration methods were consistent with those mentioned above. Overall, the body weight of each group was found to be stable, suggesting that Do-AuNPs had no significant side effects while exhibiting anti-tumor activity (Figure 6(A)). Figure 6(B) shows the growth in tumor volume throughout the experiment. The tumors in the i.p. group grew slowly, and Do-AuNPs had the strongest inhibitory effect on the tumors, which gradually shrank after approximately 10 days, while others grew in the control group. Similarly, after the mice were sacrificed, the tumor images (Figure 6(C)) and tumor weight values (Figure 7(A)) were compared with the previous results. In general, the therapeutic effect of Do-AuNPs in the i.p. group was significantly better than that of the other groups.

The i.p. administration method showed the best efficacy, which was probably related to higher and persistent drug absorption into the blood through the omentum majus. However, it contradicted the results of a previous study (Hsieh et al., 2011), which demonstrated that i.p. was more effective compared with others. Theoretically, an intramural injection (i.t.) would have a stronger anti-tumor effect than

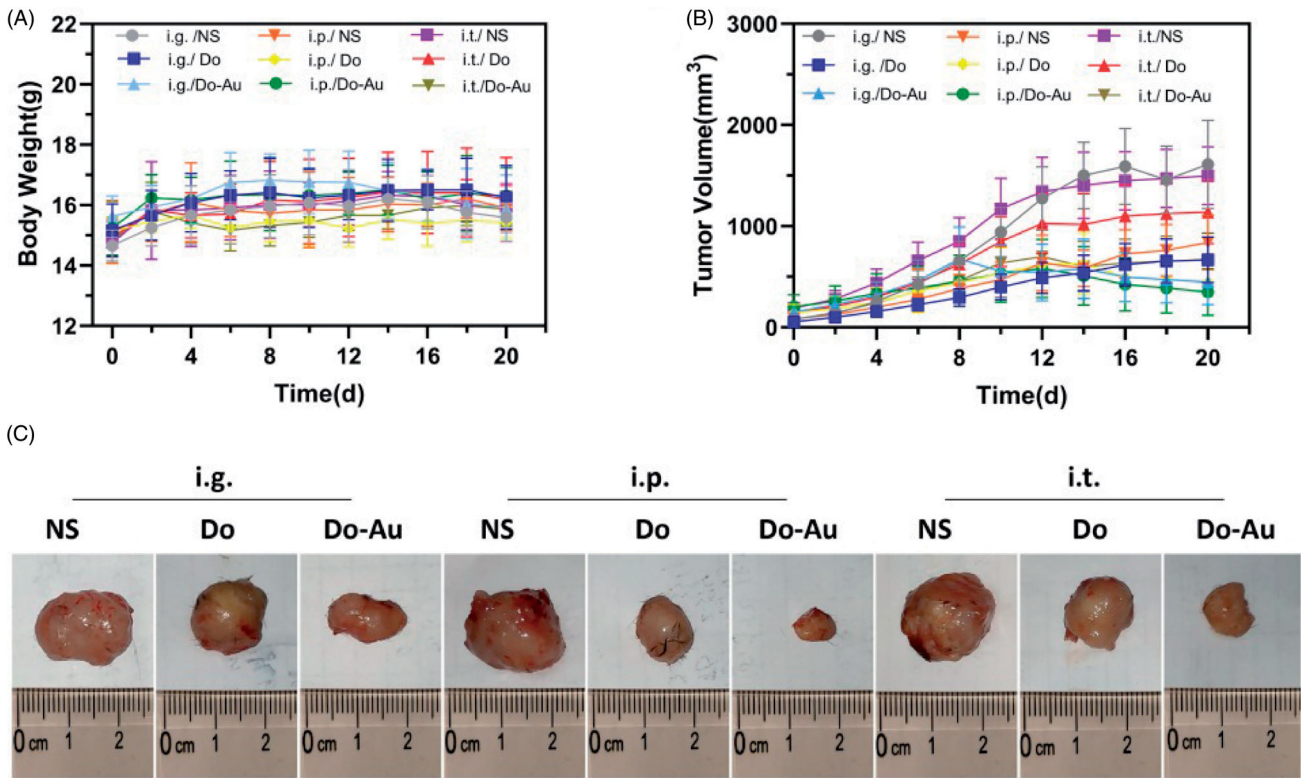


**Figure 6.** Gross tumor index. (A) Body weights during the 20 days. (B) Time-dependent tumor volume curves of different groups. (C) Photographs of tumors from nine different groups.

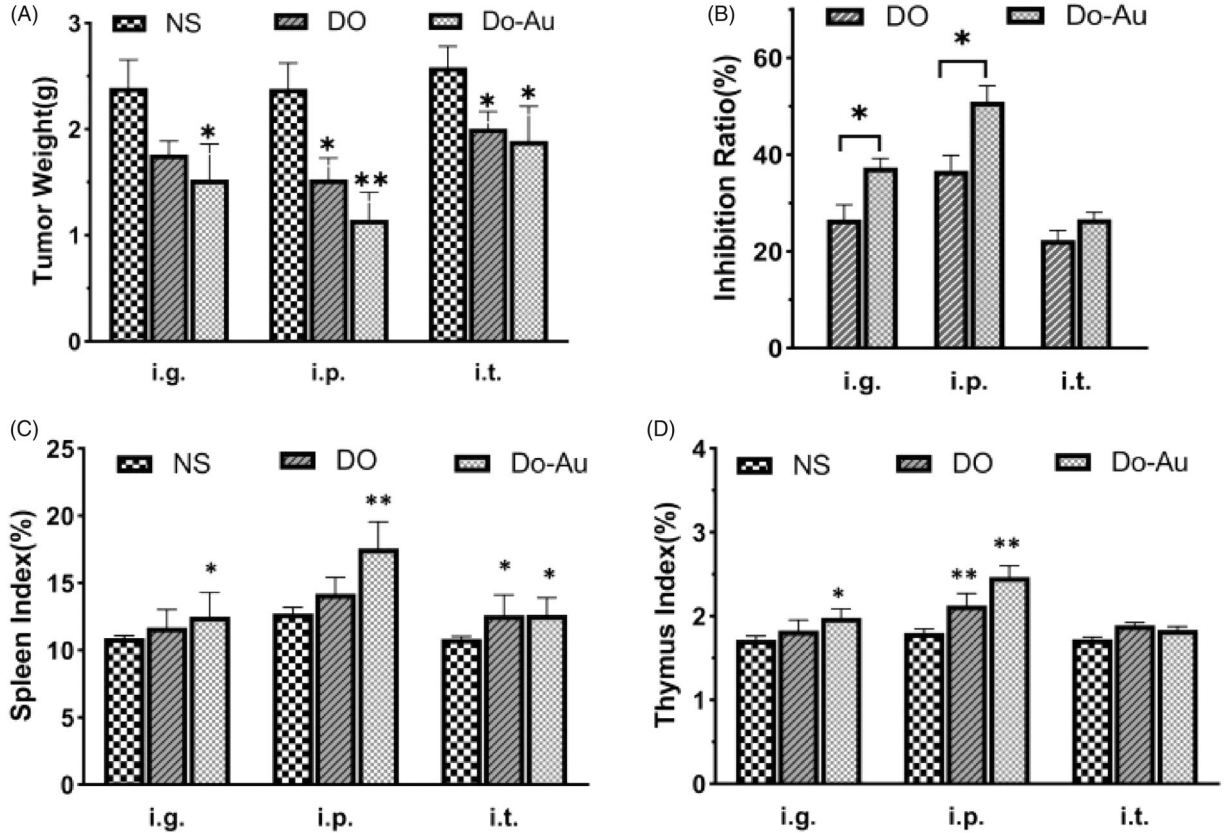


**Figure 7.** Tumor Index *in vivo*. (A) Tumor weights variability. (B) Inhibition ratio caused by treatments. (C, D) Spleen and thymus indexes of different groups. \* $p < .05$ , \*\* $p < .01$  compared to the control.

other methods because of its high concentration locally. Thus, we suggested the following reasons for the lower efficacy of i.t. in our study. First, there was always medication coming out of the pinhole even if we were careful. Additionally, the anti-tumor mechanism of Do-AuNPs did not kill the tumor cells directly but via the activation of other pathways, for instance, immune regulation. However, these hypotheses need further verification.

### 3.3.2. Spleen index and thymus index

As expected, the tumor weight inhibition rate in the Do-AuNPs group was higher than that of DO alone in all the three methods of administration (Figure 7(B)). In addition, we found that the spleen index and thymus index increased in both DO and Do-AuNPs groups, and it was comparatively higher in the Do-AuNPs group (Figure 7(C,D)). As mentioned before, the mechanism of anti-cancer effect needs further discussion. A study showed that polysaccharides from DO showed preliminary antioxidant and anti-cancer activities on HepG2 cells (Xing et al., 2018a). Another study investigated the role of isoviolanthin extracted from DO and confirmed that it inhibited the growth of HCC cells by altering the expression of EMT markers via regulating the TGF- $\beta$ /Smad and PI3K/Akt/mTOR signaling pathways (Xing et al., 2018b). What is more, DO have been shown to enhance immunity through humoral immunity or cellular immunity in mice (Liu et al., 2020). In this study, the spleen and thymus indexes of mice were increased, and the apoptotic index was higher, whereas the proliferative index was lower than other groups. Thus, we suspected that more pathways might be involved in the anti-cancer mechanism of Do-AuNPs, which needs further confirmation.

### 3.3.3. Immunohistochemical analysis

Additionally, we performed H&E, TUNEL, and Ki-67 staining of the tumor to further illustrate the efficacy of the Do-AuNPs (Figure 8(A)). The results of H&E staining in Do-AuNPs group showed more necrosis and nuclear pyknosis. Positive cells were also higher in the TUNEL and Ki-67 samples in the Do-AuNPs group compared with other groups. Similarly, the apoptotic index and proliferative index showed the same trend in the Do-AuNPs group (Figure 8(B,C)). These histological results indicated that the Do-AuNPs that were administered i.p. had stronger anti-cancer activity than other groups which was consistent with the previous results.

### 3.4. Material biosafety

The blood analysis of hepatic and renal function (ALT, AST, BUN, and CRE) was done to verify the biological safety of Do-AuNPs. Among all groups, all the indexes were within the normal range for mice (Dicson et al., 2015), and all the biochemical results showed no obvious functional damage of the liver and kidney (Figure 9(A-D)). Subsequently, H&E staining of the heart, liver, spleen, lung, and kidney was done. Do-AuNPs did not present obvious toxicity and side effects on the vital organs of the mice (Figure 10). These results indicated good biosafety of Do-AuNPs which was consistent with the results *in vitro*. Above all, our study provided a strong possibility to use the green synthesized material in cancer therapy.

## 4. Conclusions

Thus, we successfully synthesized AuNPs from TCM herbal extracts and demonstrated their inhibitory effect on liver

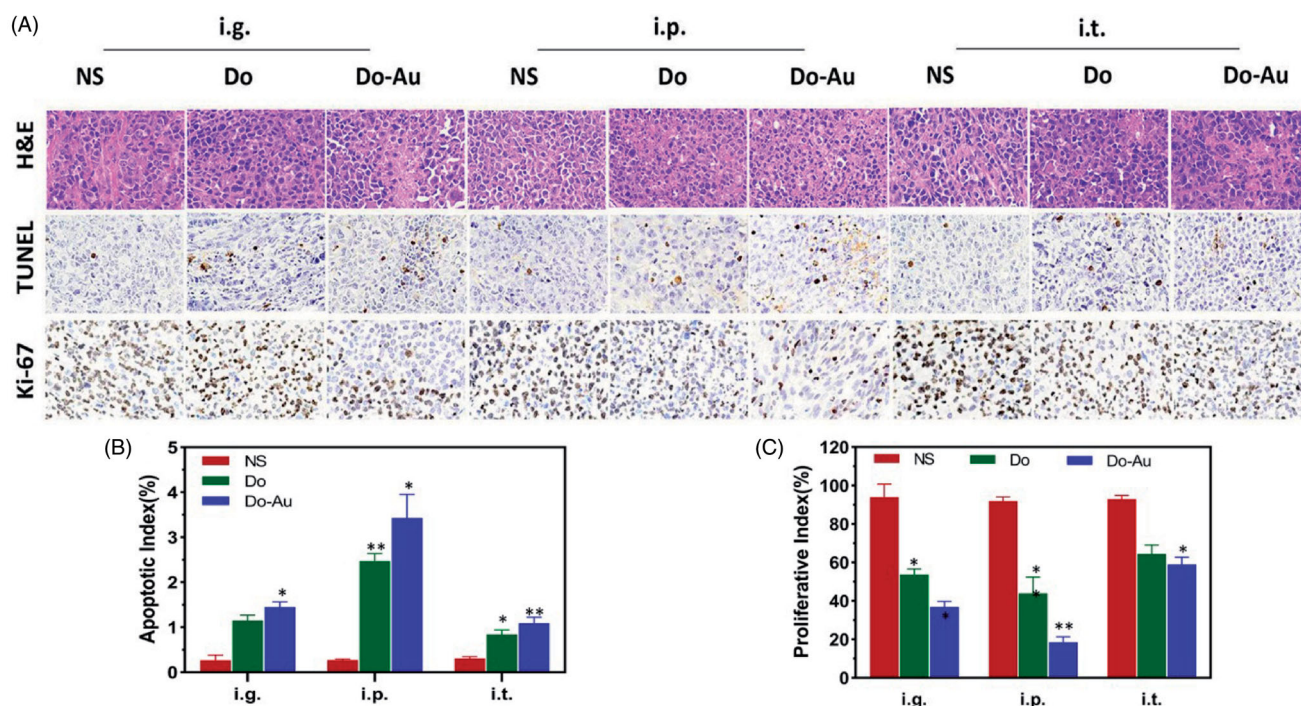


Figure 8. Histological index. (A) H&E, TUNEL, and Ki-67 staining of tumor. (B) Apoptotic index. (C) Proliferative index (\* $p < .05$ , \*\* $p < .01$  compared to the control).

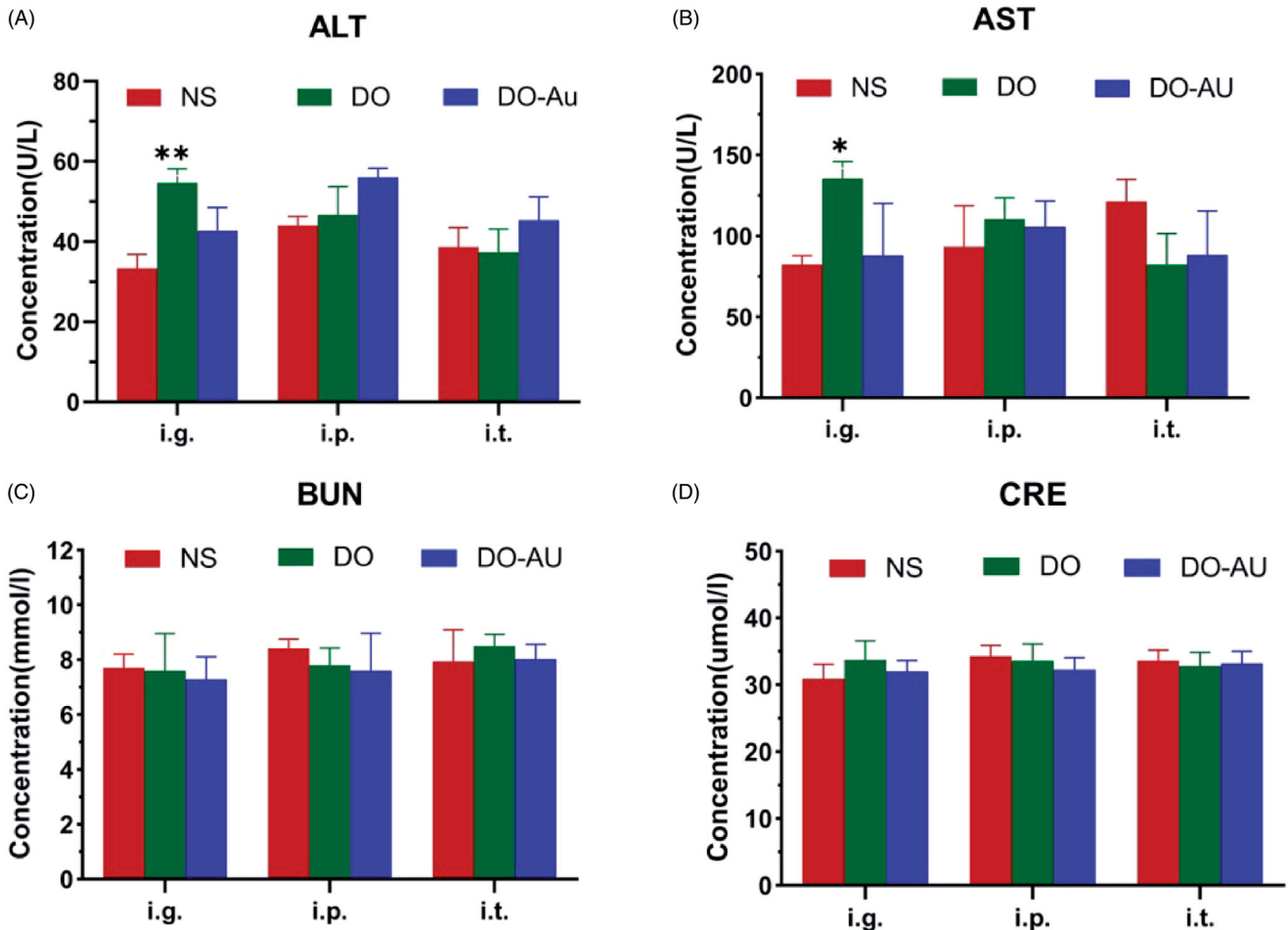


Figure 9. Bio-safety of material. (A–D) The blood biochemical analysis of ALT, AST, BUN, and CRE, respectively. \* $p < .05$ , \*\* $p < .01$  compared to the control.

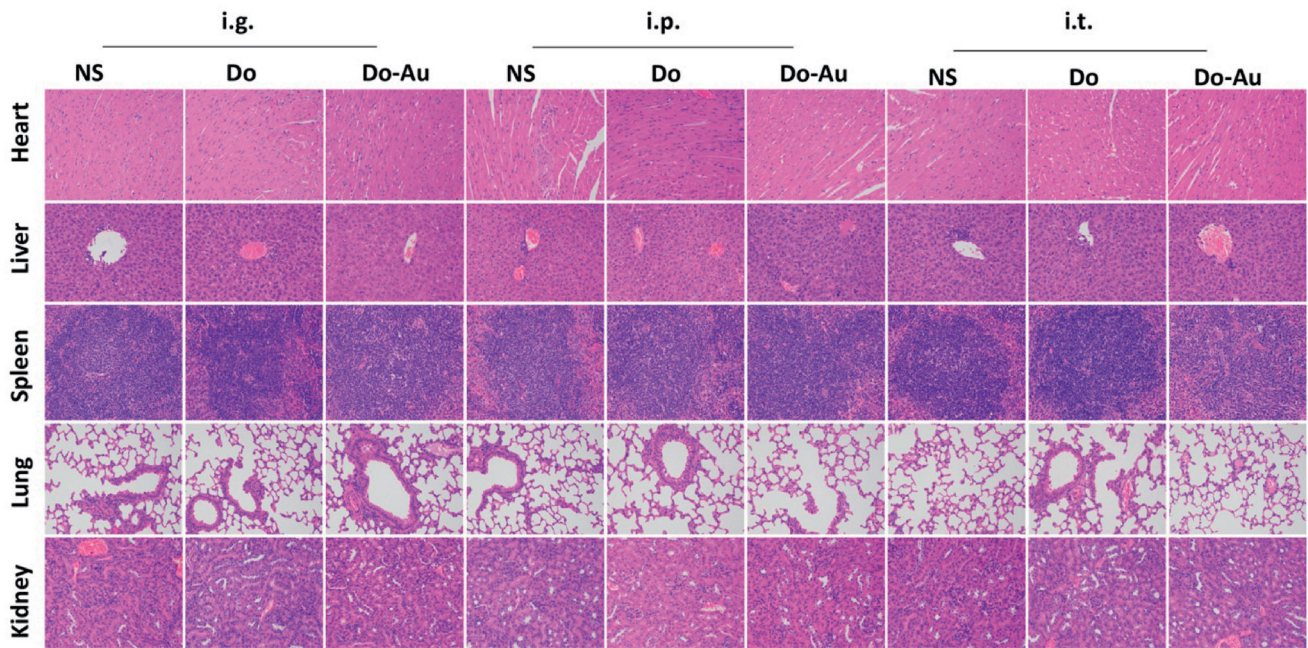


Figure 10. H&E staining photos of heart, liver, spleen, lung, and kidney in every treatment groups.



cancer *in vitro* and *in vivo*. In the process of synthesis of Do-AuNPs, the optimal conditions were 2.4 mg/mL of DO extract at 80 °C for 30 min. Then, the methods TEM, DLS, EDAX, AFM, and FTIR were used to determine the morphology, size, and composition of Do-AuNPs which were spherical shape with a size of 30 nm. Besides, the amount of DO extract on the AuNPs was calculated as 13%. *In vitro*, the inhibitory effect on HepG2 and protective effect on L02 cells of Do-AuNPs were verified by the CCK8 assay. *In vivo*, the anti-cancer activity of Do-AuNPs was preliminarily shown by a decrease in body weight and tumor volume, as well as the tumor inhibition rate. Additionally, Ki-67 and TUNEL assays were performed on the tumor for further confirmation of the inhibitory effect of Do-AuNPs on tumor. Moreover, i.p. injection has been proved to be an effective administration compared with i.g. and i.t. The biosafety of Do-AuNPs was illustrated by serum levels of ALT, AST, BUN, and CRE of mice and H&E staining of the heart, liver, spleen, lung, and kidney. Therefore, Do-AuNPs were synthesized via an environmentally friendly method that combined TCM with nanomedicine and possessed potential anti-cancer activity both *in vivo* and *in vitro*.

## Acknowledgements

The authors would like to thank all the reviewers who participated in the review and MJEditor ([www.mjeditor.com](http://www.mjeditor.com)) for its linguistic assistance during the preparation of this manuscript.

**Ethics statement:** All animal experiments and procedures were followed under guidelines authorized by the Institutional Animal Care and Use Committee of Chongqing Medical University. The research on *D. officinale* was carried out in accordance with regulations of the Central Laboratory of Second Affiliated Hospital of Chongqing Medical University. Besides, voucher specimens were authenticated by Professor Xiaojun Sun and deposited in Beijing Huadafangke Commodity Quality Inspection Co. Ltd. to access.

## Disclosure statement

The authors declare no potential conflicts of interest in this paper.

## Funding

This work was supported by the National Natural Science Foundation of China [No. 81773940 and No. 81473388].

## References

- Bagheri S, Yasemi M, Safaie-Qamsari E, et al. (2018). Using gold nanoparticles in diagnosis and treatment of melanoma cancer. *Artif Cells Nanomed Biotechnol* 46:462–71.
- Dicson SM, Samuthirapandi M, Govindaraju A, Kasi PD. (2015). Evaluation of *in vitro* and *in vivo* safety profile of the Indian traditional medicinal plant *Grewia tiliaefolia*. *Regul Toxicol Pharmacol* 73:241–7.
- Donoso-González O, Lodeiro L, Aliaga ÁE, et al. (2021). Functionalization of gold nanostars with cationic  $\beta$ -cyclodextrin-based polymer for drug co-loading and SERS monitoring. *Pharmaceutics* 13:261.
- El-Sayed IH, Huang X, El-Sayed MA. (2005). Surface plasmon resonance scattering and absorption of anti-EGFR antibody conjugated gold nanoparticles in cancer diagnostics: applications in oral cancer. *Nano Lett* 5:829–34.
- Forner A, Reig M, Bruix J. (2018). Hepatocellular carcinoma. *Lancet* 391:1301–14.
- Haiss W, Thanh NT, Aveyard J, Fernig DG. (2007). Determination of size and concentration of gold nanoparticles from UV-vis spectra. *Anal Chem* 79:4215–21.
- Hsieh DS, Wang H, Tan S-W, et al. (2011). The treatment of bladder cancer in a mouse model by epigallocatechin-3-gallate-gold nanoparticles. *Biomaterials* 32:7633–40.
- Hu J, Huang W, Zhang F, et al. (2020). Variability of volatile compounds in the medicinal plant *Dendrobium officinale* from different regions. *Molecules* 25:5046.
- Keating GM. (2017). Sorafenib: a review in hepatocellular carcinoma. *Target Oncol* 12:243–53.
- Khan MA, Khan MJ. (2018). Nano-gold displayed anti-inflammatory property via NF- $\kappa$ B pathways by suppressing COX-2 activity. *Artif Cells Nanomed Biotechnol* 46:1149–58.
- Lee MS, Ryou B-Y, Hsu C-H, et al. (2020). Atezolizumab with or without bevacizumab in unresectable hepatocellular carcinoma (GO30140): an open-label, multicentre, phase 1b study. *Lancet Oncol* 21:808–20.
- Li L, Yao H, Li X, et al. (2019). Destiny of *Dendrobium officinale* polysaccharide after oral administration: indigestible and nonabsorbing, ends in modulating gut microbiota. *J Agric Food Chem* 67:5968–77.
- Liang J, Li H, Chen J, et al. (2019). *Dendrobium officinale* polysaccharides alleviate colon tumorigenesis via restoring intestinal barrier function and enhancing anti-tumor immune response. *Pharmacol Res* 148:104417.
- Liu C-Z, Chen W, Wang M-X, et al. (2020). *Dendrobium officinale* Kimura et Migo and American ginseng mixture: a Chinese herbal formulation for gut microbiota modulation. *Chin J Nat Med* 18:446–59.
- Liu R, Pei Q, Shou T, et al. (2019). Apoptotic effect of green synthesized gold nanoparticles from *Curcuma wenyujin* extract against human renal cell carcinoma A498 cells. *Int J Nanomedicine* 14:4091–103.
- Liu Y, Song X, Cao F, et al. (2020). Banana peel-derived dendrite-shaped Au nanomaterials with dual inhibition toward tumor growth and migration. *Int J Nanomedicine* 15:2315–22.
- Lo CM, Ngan H, Tso W-K, et al. (2002). Randomized controlled trial of transarterial lipiodol chemoembolization for unresectable hepatocellular carcinoma. *Hepatology* 35:1164–71.
- Long T, Liu Z, Shang J, et al. (2018). *Polygonatum sibiricum* polysaccharides play anti-cancer effect through TLR4-MAPK/NF- $\kappa$ B signaling pathways. *Int J Biol Macromol* 111:813–21.
- Markus J, Wang D, Kim Y-J, et al. (2017). Biosynthesis, characterization, and bioactivities evaluation of silver and gold nanoparticles mediated by the roots of Chinese herbal *Angelica pubescens* Maxim. *Nanoscale Res Lett* 12:46.
- Medley CD, Smith JE, Tang Z, et al. (2008). Gold nanoparticle-based colorimetric assay for the direct detection of cancerous cells. *Anal Chem* 80:1067–72.
- Pestov A, Nazirov A, Privar Y, et al. (2016). Role of Au(III) coordination by polymer in "green" synthesis of gold nanoparticles using chitosan derivatives. *Int J Biol Macromol* 91:457–64.
- Pinato DJ, Guerra N, Fessas P, et al. (2020). Immune-based therapies for hepatocellular carcinoma. *Oncogene* 39:3620–37.
- Siegel RL, Miller KD, Fuchs HE, Jemal A. (2021). Cancer statistics, 2021. *CA Cancer J Clin* 71:7–33.
- Teng L, Yang M, Jin X, et al. (2020). Protective effect of compound formula rehmannia against neurotoxicity and apoptosis induced by  $\alpha$ -syn in *in vivo* and *in vitro* models of Parkinson's disease. *Evid Based Complement Alternat Med* 2020:5201912.
- Venkatesan J, Manivasagan P, Kim S-K, et al. (2014). Marine algae-mediated synthesis of gold nanoparticles using a novel *Ecklonia cava*. *Bioprocess Biosyst Eng* 37:1591–7.
- Wu F, Zhu J, Li G, et al. (2019). Biologically synthesized green gold nanoparticles from Siberian ginseng induce growth-inhibitory effect on melanoma cells (B16). *Artif Cells Nanomed Biotechnol* 47:3297–305.
- Xie SZ, Liu B, Zhang D-D, et al. (2016). Intestinal immunomodulating activity and structural characterization of a new polysaccharide from stems of *Dendrobium officinale*. *Food Funct* 7:2789–99.

- Xing S, Yu W, Zhang X, et al. (2018b). Isoviolanthin extracted from *Dendrobium officinale* reverses TGF-beta1-mediated epithelial-mesenchymal transition in hepatocellular carcinoma cells via deactivating the TGF-beta/Smad and PI3K/Akt/mTOR signaling pathways. *Int J Mol Sci* 19:1556.
- Xing S, Zhang X, Ke H, et al. (2018a). Physicochemical properties of polysaccharides from *Dendrobium officinale* by fractional precipitation and their preliminary antioxidant and anti-HepG2 cells activities in vitro. *Chem Cent J* 12:100.
- Yang J, Chen H, Nie Q, et al. (2020). *Dendrobium officinale* polysaccharide ameliorates the liver metabolism disorders of type II diabetic rats. *Int J Biol Macromol* 164:1939–48.
- Yang X, Wang D, Lin J, et al. (2020). Atezolizumab plus bevacizumab for unresectable hepatocellular carcinoma. *Lancet Oncol* 21:e412.
- Yau T, Hsu C, Kim T-Y, et al. (2019). Nivolumab in advanced hepatocellular carcinoma: sorafenib-experienced Asian cohort analysis. *J Hepatol* 71:543–52.
- Yu Y, Shen M, Song Q, Xie J. (2018). Biological activities and pharmaceutical applications of polysaccharide from natural resources: a review. *Carbohydr Polym* 183:91–101.
- Zhang S, Pang G, Chen C, et al. (2019). Effective cancer immunotherapy by *Ganoderma lucidum* polysaccharide-gold nanocomposites through dendritic cell activation and memory T cell response. *Carbohydr Polym* 205:192–202.
- Zhang X, Tan Z, Jia K, et al. (2019). *Rabdosia rubescens* Linn: green synthesis of gold nanoparticles and their anticancer effects against human lung cancer cells A549. *Artif Cells Nanomed Biotechnol* 47: 2171–8.
- Zhou C, Xie Z, Lei Z, et al. (2018). Simultaneous identification and determination of flavonoids in *Dendrobium officinale*. *Chem Cent J* 12:40.
- Zou S, Duan B, Xu X. (2019). Inhibition of tumor growth by beta-glucans through promoting CD4(+) T cell immunomodulation and neutrophil-killing in mice. *Carbohydr Polym* 213:370–81.